

## The effects of ocean SST dipole on Mongolian summer rainfall

Hiroshi Yasuda<sup>1</sup>, Banzragch Nandintsetseg<sup>2, 4</sup>, Ronny Berndtsson<sup>3</sup>,  
Ganbat Amgalan<sup>2</sup>, Masato Shinoda<sup>4</sup> and Takayuki Kawai<sup>1</sup>

<sup>1</sup> Arid Land Research Center, Tottori University, Hamasaka, Tottori, Japan

<sup>2</sup> Information and Research Institute of Meteorology,  
Hydrology and Environment, Ulaanbaatar, Mongolia

<sup>3</sup> Centre for Middle Eastern Studies & Division of Water Resources  
Engineering, Lund University, Lund, Sweden

<sup>4</sup> Graduate School of Environmental Studies, Nagoya University, Nagoya, Japan

*Received 30 November 2016, in final form 15 May 2017*

Cross-correlations between inter-annual summer rainfall time series (June to August: JJA) for arid Mongolia and global sea surface temperatures (GSST) were calculated for prediction purposes. Prediction of summer rainfall for four vegetation zones, Desert Steppe (DS), Steppe (ST), Forest Steppe (FS), and High Mountain (HM) using GSSTs for time lags of 5, 6, and 7 months prior to JJA rainfall was evaluated. Mongolian summer rainfall is correlated with global SSTs. In particular, the summer rainfall of FS and HM displayed high and statistically significant correlations with SST in specific parts of the oceans. SST dipoles (pairs of positively and negatively correlated areas) were identified, and correlation for time series of the SST differences between SST dipoles (positive – negative) with the summer rainfall time series was larger than the original correlations. To predict the summer rainfall from SST, an artificial neural network (ANN) model was used. Time series of the SST difference that represents the strength of the dipole were used as input to the ANN model, and Mongolian summer rainfall was predicted 5, 6, and 7 months ahead in time. The predicted summer rainfall compared reasonably well with the observed rainfall in the four different vegetation zones. This implies that the model can be used to predict summer rainfall for the four main Mongolian vegetation zones with good accuracy.

*Keywords:* artificial neural network, dryland, Mongolian rainfall, rainfall prediction, SST teleconnection

### 1. Introduction

Sea surface temperature (SST) teleconnections are today well known to initiate global climate anomalies (*e.g.*, Uvo et al., 1998; Elagib et al., 2011; Fontaine et al., 2011; Rodriguez-Fonseca et al., 2006; Ahmed et al., 2008; Nagano et al.,

2009). The El Niño Southern Oscillation (ENSO) is such a phenomenon often used to predict weather anomalies. Both El Niño (warmer SST) and La Niña (cooler SST) initiate unusual weather globally (*e.g.*, Elagib et al., 2011; Fontaine et al., 2011; Osman et al., 2002; Davig et al., 2006; Diro et al., 2011; Mondal et al., 2011; Kumbuyo et al., 2014). Along with the ENSO in the Pacific Ocean, also the Indian Ocean SST dipole is a well-known sea-atmospheric climatic indicator for weather anomalies. The Indian Ocean SST dipole is defined as the SST difference between the tropical western Indian Ocean (50–70° E, 10° S–10° N) and the tropical southeastern Indian Ocean (90° E–110° E, 10° S–equator). A positive phase is defined as cold eastern and warm southwestern areas that initiate strong wind anomalies. The Indian Ocean initiated wind anomalies relate to climate conditions, particularly in Africa (Camberlin et al., 1997; Saji et al., 1999; Webster et al., 1999; Yu et al., 1999; Iizuka et al., 2000; Ashok et al., 2001; Behera et al., 2001).

At a global scale, SST differences between the hemispheres initiate a change in the atmospheric meridional heat transport and excite rainfall in the tropics (*e.g.*, Mantsis and Clement 2009). The equatorial zonal SST gradient in the Pacific Ocean is defined as the SST averaged over 5° N–5° S and 130° E–200° E subtracted from the SST averaged over 5° S–5° N and 200° E–270° E (the SST of the eastern section minus that of the western section) as an indication of such inter-hemispheric thermal gradients (Chiang et al., 2008). The equatorial zonal SST gradient strengthens with an increased northward inter-hemispheric thermal gradient. Simulation results indicate that the hemispheric SST gradient promotes dry climate in the Sahel (Biasutti and Giannini, 2006). A multi-decadal latitudinal shift in the branch of the Hadley Cell and precipitation in the tropics was demonstrated by simulations (Mantsis and Clement, 2009). These are well correlated with the inter-hemispheric SST difference. The zonal SST gradient promotes the inter-hemispheric thermal gradient in the northern direction.

The East Asian summer monsoon rainfall (JJA) and dipoles (positively and negatively correlated areas) over the Pacific Ocean are linked (Chiang et al., 2008). The SST links with the ocean heat content were applied to a linear regression model for prediction of summer rainfall. Results of model experiments showed that the effect of the meridional SST gradient on land precipitation is more significant than an overall tropical warming (Chung and Ramanathan 2007). The summer monsoon in East Asia is subject to the difference between the SST anomaly of the North Pacific (120°–160° E, 36°–44° N) and the Indo–Pacific warm pool (80°–130° E, 4°–24° N) (Zheng et al., 2014). These two SST zones are defined as the North Pacific Ocean dipole. The SST difference between the two SST regions over the Bay of Bengal is associated with convection and consequent rainfall events during the monsoon season (Shankar et al., 2007). Link of hydro-meteorological condition in Mongolia with Pacific Ocean variations such as Pacific decadal oscillation (PDO) and ENSO was reported by Davi et al. (2006). Mongolian cyclone is indicated by large fluctuation of East Asian Summer

Monsoon and preceded with the pattern of SST anomalies over the eastern tropical Pacific Ocean (Sun et al., 2017).

As explained above, the SST difference between two areas defines a thermal gradient that initiates wind and weather anomalies. Thus, the SST difference is often used as a predictor of climate anomalies. In view of this, our objective is to investigate the teleconnections of SST dipole differences over the oceans with Mongolian summer rainfall. If these teleconnections are strong, they can be used to predict rainfall several months ahead in time by using the observed SST dipole differences.

## 2. Study area and data

Mongolia lies in a transitional zone (42°–52° N) between the boreal forests of Siberia and the Gobi Desert, spanning the southernmost border of the area of permafrost and the northernmost deserts of Central Asia (Fig. 1). About half of Mongolia lies at an altitude of about 1400 m a.m.s.l., making it one of the countries with the highest elevation in the world. Because of its geographical and topographical characteristics, Mongolia has a cold and arid climate. Precipitation decreases and temperature (and consequently evapotranspiration) increases southward, resulting in increasingly arid conditions. More than 40% of Mongolia is arid or hyper-arid. Mongolia typically has a long, cold, dry winter (Siberian winter) and a short, warm summer (Goulden et al., 2011, 2016).

Summer precipitation variability is a key factor driving pasture production, livestock dynamics, and human subsistence in the dry and cold climate of Mongolia, and it has caused a significant amount of damage to the economy and society. The pasture production of Mongolia is the basis for the nutrition of approximately 52 million head of livestock, which is the livelihood basis of the country's rural population (Nandintsetseg and Shinoda, 2014). For improved planning and management of pasture, it is necessary to predict summer precipitation as part of a drought early warning system.

The region's location, size, and topography have resulted in a unique assembly of natural vegetation zones (Fig. 1). The northernmost zone consists of taiga forest and forest steppe, while the southern region contains steppe, desert steppe, and desert. The northern part of Mongolia is covered by forested mountain ranges with a dry sub-humid climate, whereas the southern part encompasses the Gobi Desert at lower elevations with a drier climate (Nandintsetseg and Shinoda, 2011). In this study, we used monthly precipitation data collected from twelve stations well distributed across Mongolia during the period 1979–2013. The twelve stations were selected as representative for the four major vegetation zones: desert steppe (DS), steppe (ST), forest steppe (FS), and high mountain (HM), as shown in Fig. 1. The precipitation data were taken from the Institute of

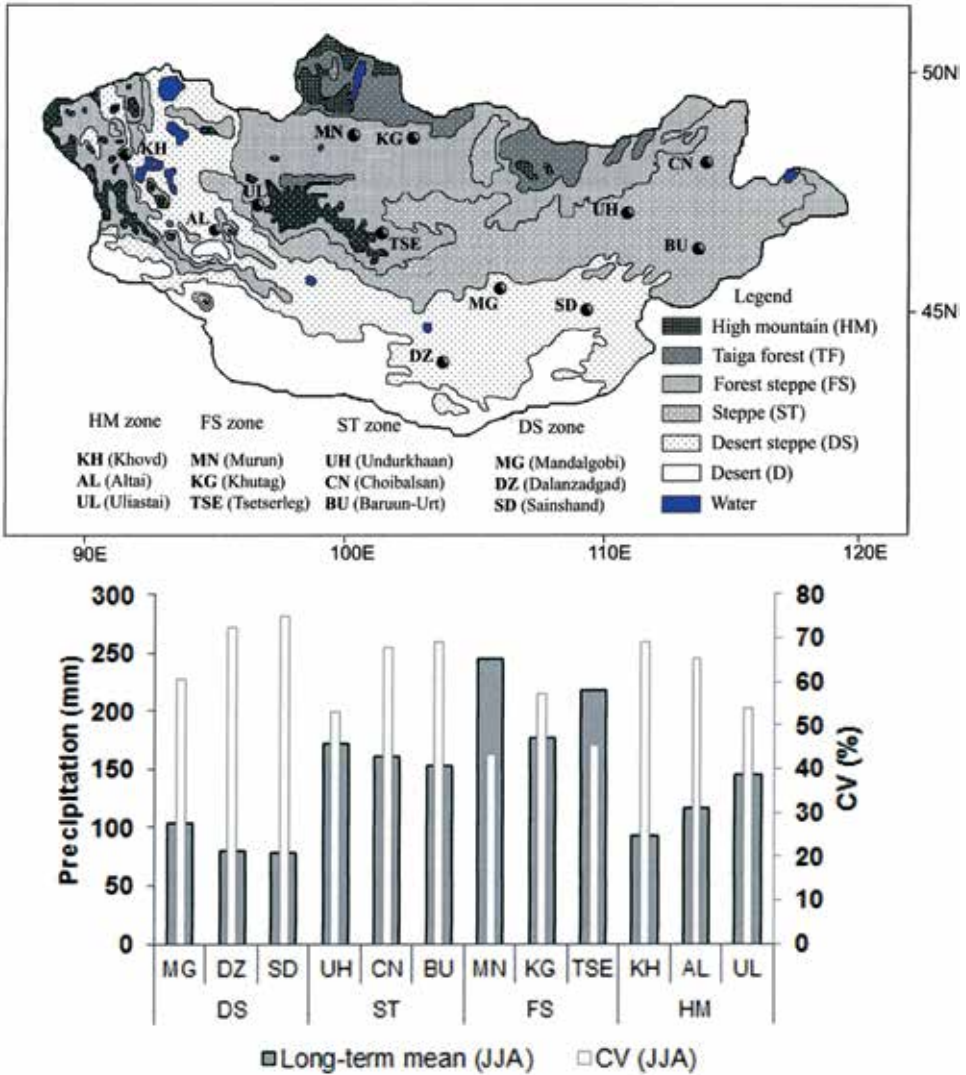


Figure 1. Vegetation zones in Mongolia. Summer rainfall for the four major vegetation zones, namely desert steppe (DS), steppe (ST), forest steppe (FS), and high mountain (HM), was investigated in this paper (above). Mean precipitation and CV of stations (below).

Meteorology, Hydrology and Environment of Mongolia (IMHE). Each vegetation zone was represented by three rainfall stations.

In general, annual precipitation ranges from over 400 mm in the northern mountains to below 100 mm in the south and is concentrated during the summer months (June–August). Mean annual precipitation amounts for the DS, ST, FS, and HM zones are 129.3, 243.2, 305.9, and 141.4 mm, respectively. The

coefficient of variation (*CV*) for the annual precipitation for the four zones are 0.239, 0.236, 0.153, and 0.269, respectively. The annual mean temperature is approximately  $-4\text{ }^{\circ}\text{C}$  in the high mountains,  $2\text{ }^{\circ}\text{C}$  in the steppe and desert steppe zones, and  $6\text{ }^{\circ}\text{C}$  in the desert regions. Snowfall occurs between mid-October and the end of April, and the annual maximum snow depth (34 mm) occurs in January (Morinaga et al., 2003). The growing season (from May to August) in Mongolia is very short. The beginning of plant emergence and senescence occur in late April to early May and late September, respectively. It is very dependent on climate, mainly precipitation through soil moisture (Shinoda et al., 2007; Nandintsetseg and Shinoda, 2011, 2015). Averages of the monthly precipitation for the four zones are shown in Fig. 2. Inter-annual time series of summer rainfall (JJA) for the four zones are shown in Fig. 3. The summer rainfall is given as the average amount of rainfall for three month (JJA). The inter-annual means of the summer rainfall for the four zones (DS, ST, FS, and HM) are 29.1, 56.6, 71.2, and 31.5 mm, respectively. The coefficient of variation of summer rainfall in the four zones are 0.306, 0.314, 0.201, and 0.375, respectively. A consecutive

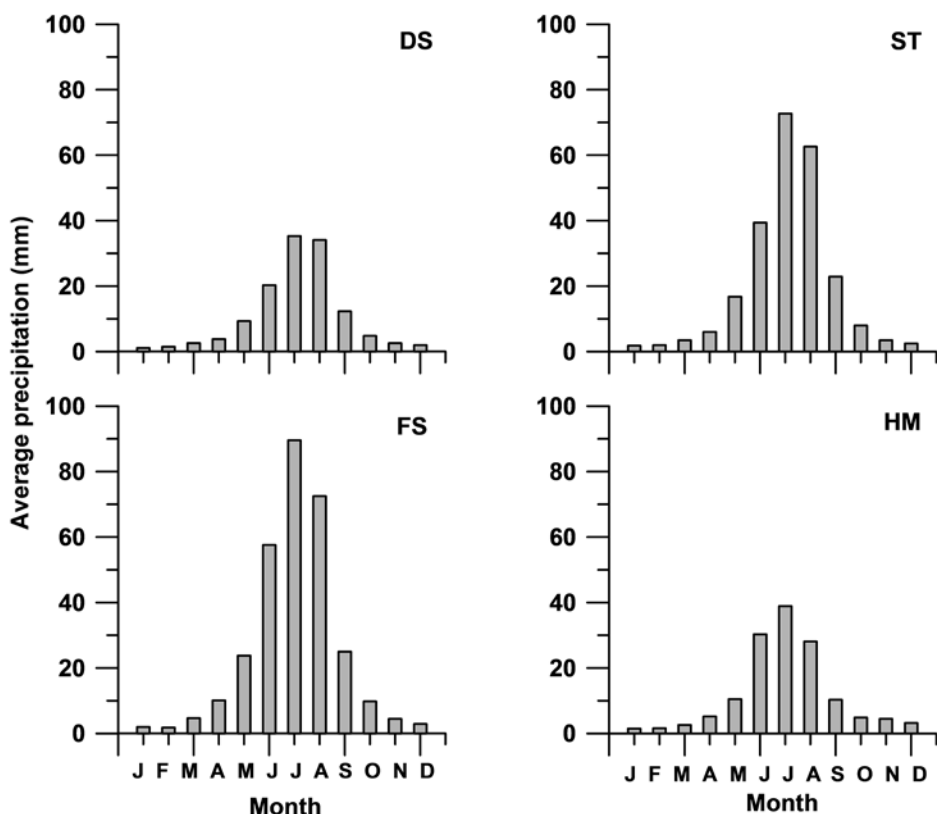


Figure 2. Monthly average rainfall for the four investigated vegetation zones.

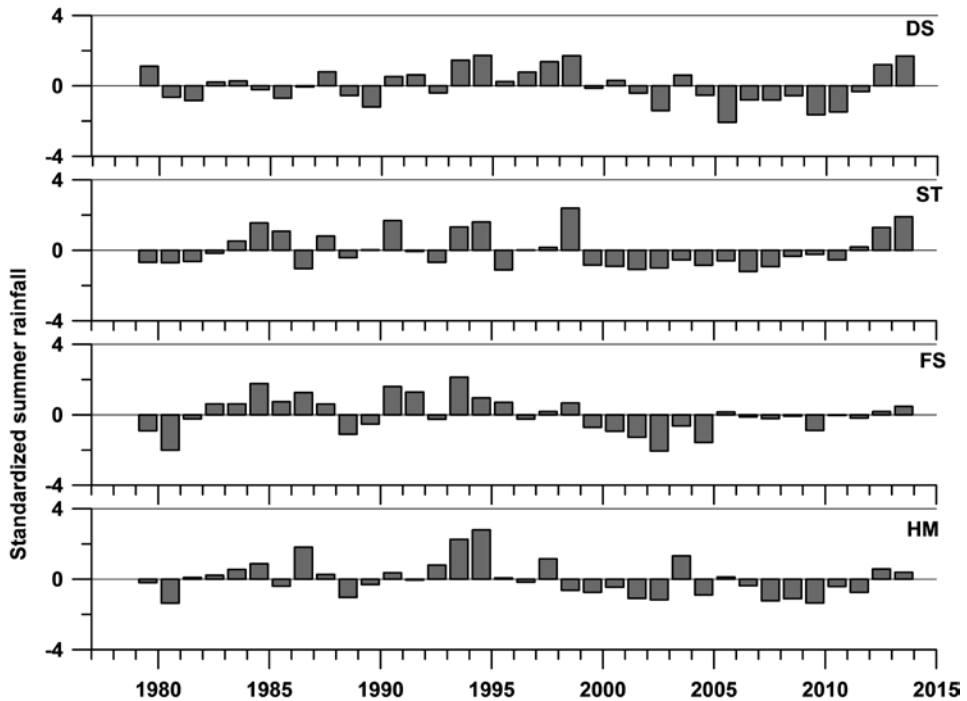


Figure 3. Standardized summer rainfall (3 months; JJA) in the four investigated vegetation zones.

tendency of wetting or drying during several few years is suggested from Fig. 3. For all four zones, wet periods were 1993–1994 and 2012–2013 and dry periods was 1988–2002.

### 3. Methodology

#### 3.1. Cross-correlation between GSST and summer rainfall

To evaluate teleconnections, cross-correlations between the mean summer rainfall (JJA) of the four zones and mean three-month SST were calculated (*e.g.*, Smith et al., 2000; Yasuda et al., 2009). For prediction purposes, we evaluated cross-correlations with time lags of 5, 6, and 7 months as reasonable lead-times. For example, with a lag of 5 months, the mean values of the SST for three months (January, February, and March: JFM) were applied for calculation of the correlation, corresponding to the summer rainfall (mean value for three months, JJA). In this case, the JFM SST could be used as a predictor of JJA rainfall if a strong correlation is found. In the results below, we consistently compare the correlation between SST and lagged JJA rainfall. Whether SST can be used to predict future summer rainfall at the different respective lag times is discussed below.

### 3.2. Artificial neural network

An artificial neural network (ANN) was used to predict rainfall, with SST as predictor. The ANN is a non-dynamic model that has often been used for time series prediction in hydrology and meteorology (*e.g.*, Bishop, 1995; Olsson et al., 2001; Srivastava et al., 2006; Srivastava et al., 2010; Singh and Borah, 2013; Dash et al., 2010). The ANN is flexible to develop and can predict highly varying physical phenomena. In this study, a three-layered ANN was used for the prediction (Yasuda et al., 2009). The three-layered ANN consists of input, hidden, and output layers. Each layer contains neurons. Neurons corresponding to time series of the SST difference and the summer rainfall form the input and output layers, respectively. The hidden layer connects the output and input layers. Weights connect neurons in each layer (between input and hidden layers and vice versa). The weights were optimized by a back propagation procedure. To obtain a better fit for the ANN, different neuron arrangements in the hidden layers were examined. For DS, ST, and HM, an arrangement of 3, 6, and 1 neurons were applied to the hidden layers and 2, 4, and 1 neurons were applied to the layers for FS. For DS, ST, and HM, inter-annual SST difference for the previous two years in addition to the present year were used and prediction started from 1981. For FS, the prediction started from 1980 as the SST difference for two years were applied to the input layer.

## 4. Results and discussion

### 4.1. Cross-correlation between GSST and summer rainfall

Figures 4-1 and 4-2 show the SST zones that indicated statistically significant correlation ( $|r| \geq 0.33$ ) with summer rainfall (JJA) for the four vegetation zones at lags of 5, 6, and 7 months.

The patterns showing correlations between SST and summer rainfall over the examined regions have higher correlation values and cover broader areas for FS and HM than those for DS and ST. These results imply that summer rainfall in inland Mongolia is teleconnected with some parts of the oceans. Both the FS and HM areas indicated significant correlation with SST over the north and tropics of the Atlantic, off the west coast of North America, south of Japan, east of Australia, off Chile in the Pacific Ocean, and over the South Indian Ocean. In particular, Atlantic Ocean SST is strongly correlated with rainfall in FS and HM. Areas showing negative correlation with all four vegetation zones are located off Greenland in the northern Atlantic Ocean. Areas showing negative correlations with all four vegetation zones are located off the west coast of North America. In general, the correlation patterns for FS and HM are nearly equivalent.

The summer rainfall of DS displays a significant positive correlation with SST areas east of the Gulf of Mexico and off the west coast of South America at

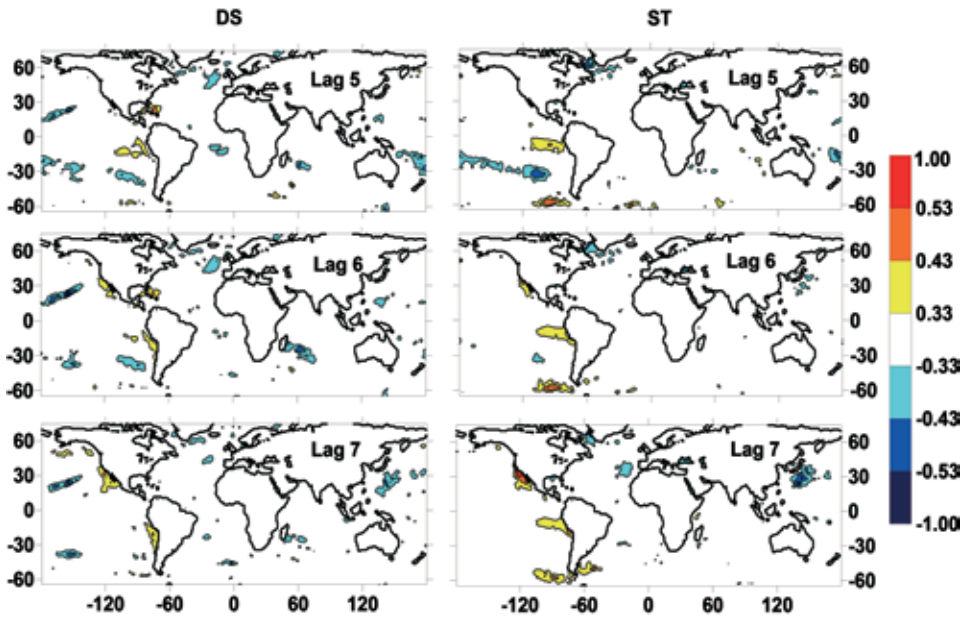


**Figure 4-1.** Summer rainfall correlation with SST (lags of 5, 6, and 7 months) for the investigated vegetation zones (DS and ST). Correlations of 0.33, 0.43, and 0.53 correspond to statistical significance levels of 0.05, 0.01, and 0.001, respectively.

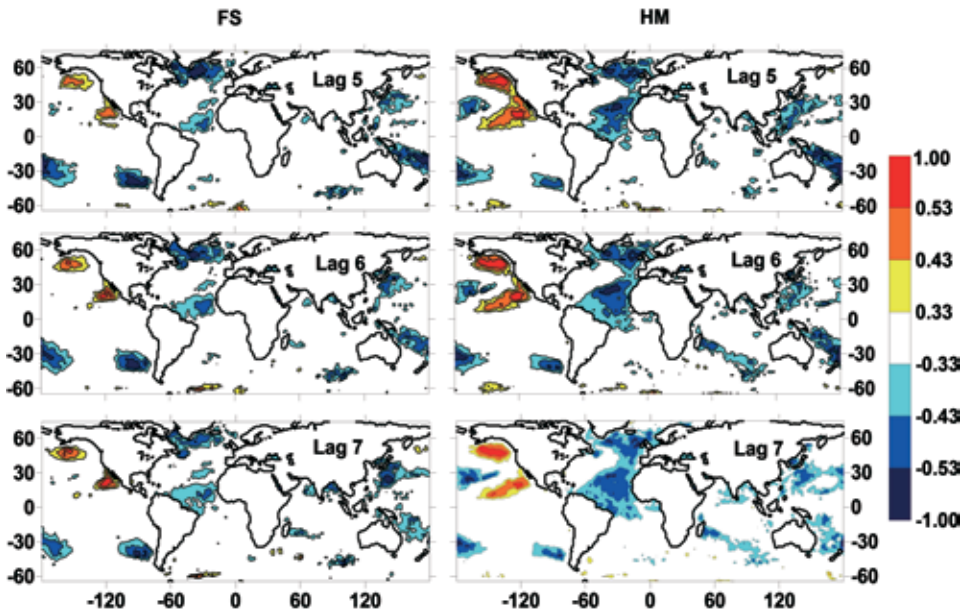


**Figure 4-2.** Summer rainfall correlation with SST (lags of 5, 6, and 7 months) for the investigated vegetation zones (FS, and HM).

lag 5–6 months. Significant negative correlations are found for SST areas west of Great Britain and east of Madagascar. Other significant negative correlations are found for sea areas near Hawaii in the Pacific Ocean for lags of 5, 6, and 7 months. For 7 months' lag, positive correlations are found for areas off the west coast of North America, and negative correlations are found over the sea south of Japan.

The ST summer rainfall displays significant positive correlations for lags of 5, 6, and 7 months with SST areas off the coast of Peru and southwest of Chile in the Pacific Ocean, suggesting that ENSO is a climatic phenomenon with potential impact on the Mongolian summer rainfall. Moreover, the area southwest of Greenland in the northern Atlantic Ocean displays positive correlation for lags 5–7 months. For a lag of 7 months, positive correlations are found with areas off the west coast of North America, and negative correlations are found south of Japan. For a lag of 5 months, negatively correlated areas spread from the sea north of New Zealand to off the coast of Chile in the Pacific Ocean.

The summer rainfall of FS is negatively correlated with sea areas south of Greenland and low latitude areas between Africa and South America in the Atlantic Ocean for 5–7 month time lag. Negatively correlated areas are also widely spread from northeast of Australia to east of New Zealand and off Chile, southeast of Japan in the Pacific Ocean, and over the South Indian Ocean. Positively correlated areas are spread over sea areas south of Alaska and off the Baja California peninsula in the Pacific Ocean. Sea areas east and south of Japan display continuous positive correlation. For lag times of 5 and 6 months, negatively correlated areas are found east of Australia.

#### *4.2. SST dipole difference*

As shown above, the summer rainfall (JJA) for the four major Mongolian vegetation zones displayed significant positive and negative correlations with various SST areas over several ocean areas. Research has shown that SST contributes to land climate in a spatially varying way and with both negative and positive correlations (Biasutti and Giannini, 2006; Chiang et al., 2008; Mantsis and Clement, 2009). The SST difference between Bay of Bengal regions is associated with convective rainfall processes (Shankar et al., 2007). For example, SST-differenced dipoles provide stronger correlation with summer rainfall over the Loess Plateau as compared to consideration of just positive or negative SSTs (Yasuda et al., 2009). Links to the summer monsoon rainfall (JJA) of East Asia (20°–50° N, 110°–145° E) with dipoles over the Pacific Ocean at 6-month time lag (DJF) were reported by Lee et al. (2008). We also selected significant dipoles to maximize the correlation and predictive ability of the relationships between SST and summer rainfall.

(i) Vegetation zone DS

Figure 5-1 shows a significant SST dipole in the Atlantic Ocean related to summer rainfall in the DS vegetation zone. The time series of SST dipole difference and corresponding summer rainfall ( $|r|>0.33$ , lag 5 months) are shown to the right. The red SST area east of Florida and the blue area west of Europe indicate positive and negative correlations with the summer rainfall, respectively. The averaged positive and negative correlations with summer rainfall were 0.51 and  $-0.40$ , respectively. The correlation for the time series of the SST difference (positive – negative) with the summer rainfall was 0.60, an increase by approximately 10%.

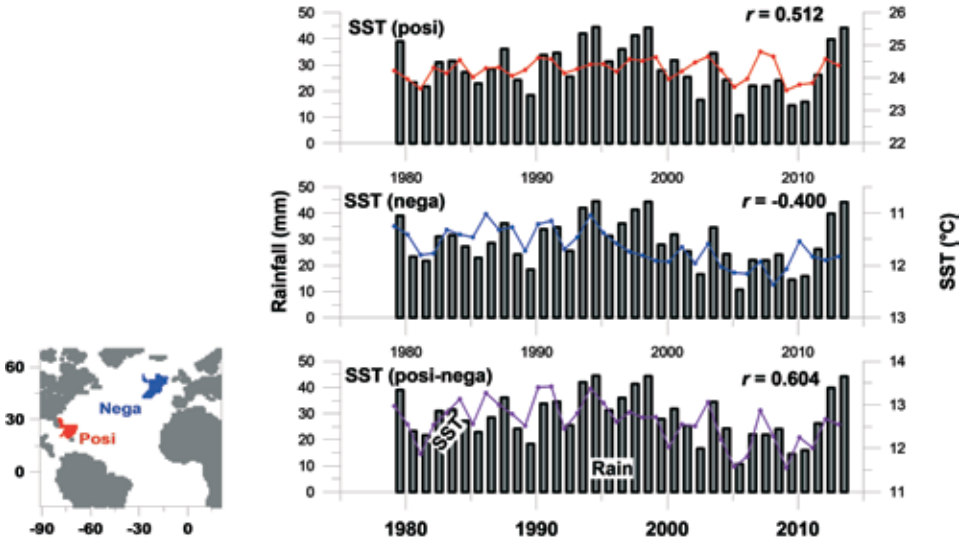


Figure 5-1. Vegetation zone DS summer rainfall significant SST dipole areas. Right: SST dipole difference and corresponding summer rainfall ( $|r|>0.33$ , lag 5 months).

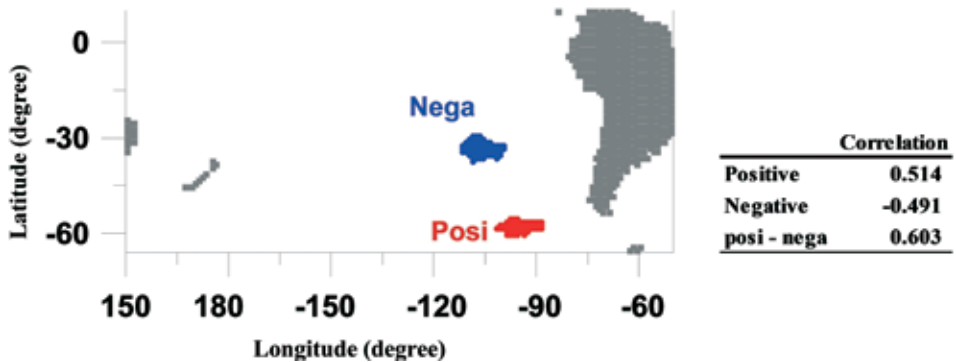


Figure 5-2. Vegetation zone ST summer rainfall significant SST dipole areas ( $|r|>0.43$ , lag 5 months).

(ii) Vegetation zone ST

Figure 5-2 shows the dipole west of Chile in the Pacific Ocean for a lag of 5 months. The negatively correlated area is located to the north, and the positively correlated area is located to the south. The positive and negative correlations of the SST with the summer rainfall of ST are 0.51 and  $-0.49$ , respectively. The correlation of the time series of the SST difference is 0.60, nearly 10% higher than the original time series.

(iii) Vegetation zone FS

For a time lag of 7 months, correlations of the spatially averaged SST dipole (positive area located south of Alaska, and negative area south of Japan) with the summer rainfall for vegetation zone FS are 0.57 and  $-0.64$ , respectively (Fig. 6-3a). The correlation of the time series of the SST dipole difference is 0.76, about 10% stronger than the original correlation (Fig. 5-3).

(iv) Vegetation zone HM

For a time lag of 5 months, the positive correlation zone is off south Alaska ( $r = 0.61$ ), and the negative zone is north of New Zealand ( $r = -0.65$ ). The correlation of the time series of the SST difference is 0.78 (Fig. 5-4).

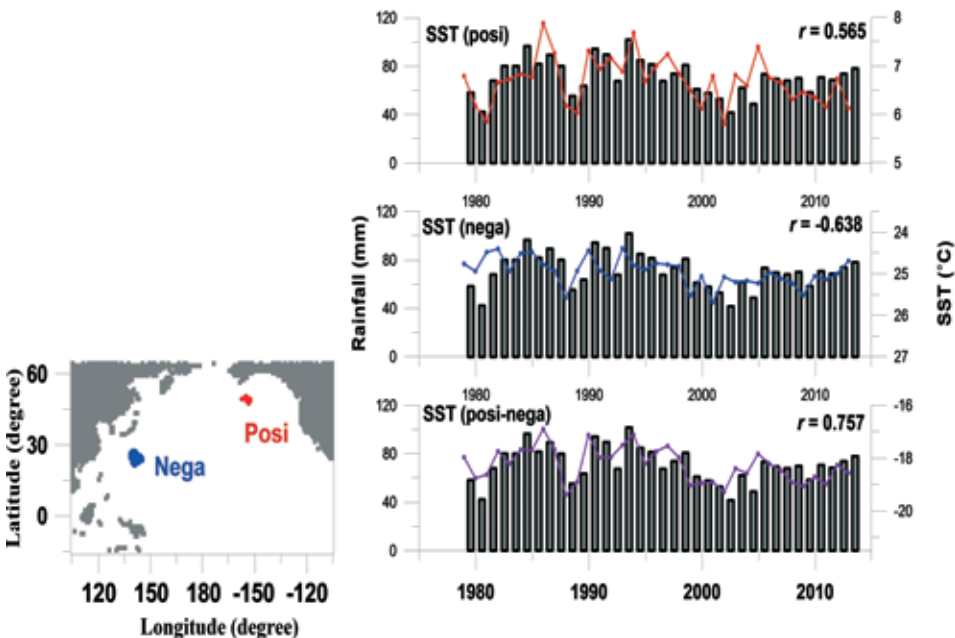


Figure 5-3. Left: Vegetation zone FS summer rainfall significant SST dipole areas. Right: Vegetation zone DS summer rainfall significant SST dipole areas ( $|r| > 0.53$ , lag 7 months).

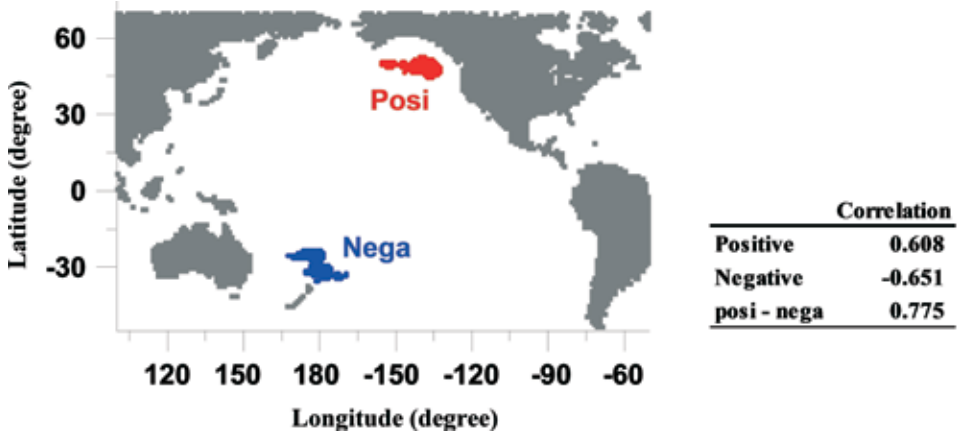


Figure 5-4. Vegetation zone HM summer rainfall significant SST dipole areas ( $|r| > 0.53$ , lag 5).

#### 4.3. General correlation between SST and summer rainfall for all vegetation zones

The general correlations (significance  $|r| \geq 0.33$ ) between GSST and summer rainfall for all four vegetation zones for lags of 5, 6, and 7 months are shown in Fig. 6. The SST areas along the south of Greenland indicate significant correlations with the summer rainfall for all four zones at consecutive lags of 5, 6, and 7 months. This implies a significant contribution from the North Atlantic Ocean SST to the summer rainfall in Mongolia. For lags of 6 and 7 months, SST zones off the west coast of North America indicate significant positive correlations. For a lag of 5 months, negatively correlated areas are scattered from the northeast of Australia to off the west coast of South America. For a lag of 6 months, a negatively correlated area is found off the west coast of South America at a lag of 5 months. For a lag of 7 months, a negatively correlated zone is located east of Madagascar in the Indian Ocean. In the Pacific Ocean, there is a dipole consisting of a negatively correlated area south of Japan and a positively correlated area off the west coast of North America. The difference of SST indicates higher correlation.

#### 4.4. General SST dipoles for all vegetation zones

When summer rainfall is considered for all four vegetation zones, a strong SST dipole is obtained with the negative correlations off the west coast of North America and with the positive correlations south of Japan for a time lag of 7 months (Fig. 7). The significance level is  $|r| \geq 0.43$  for correlation with vegetation zones DS and HM and  $|r| \geq 0.53$  for ST and FS. Figure 8 shows the summer rainfall for ST and spatial mean SST for the positive (top) and negative (middle) zones. Correlations between the SST time series with the summer rainfall are 0.61 and  $-0.58$ , respectively. The correlation between differenced time series

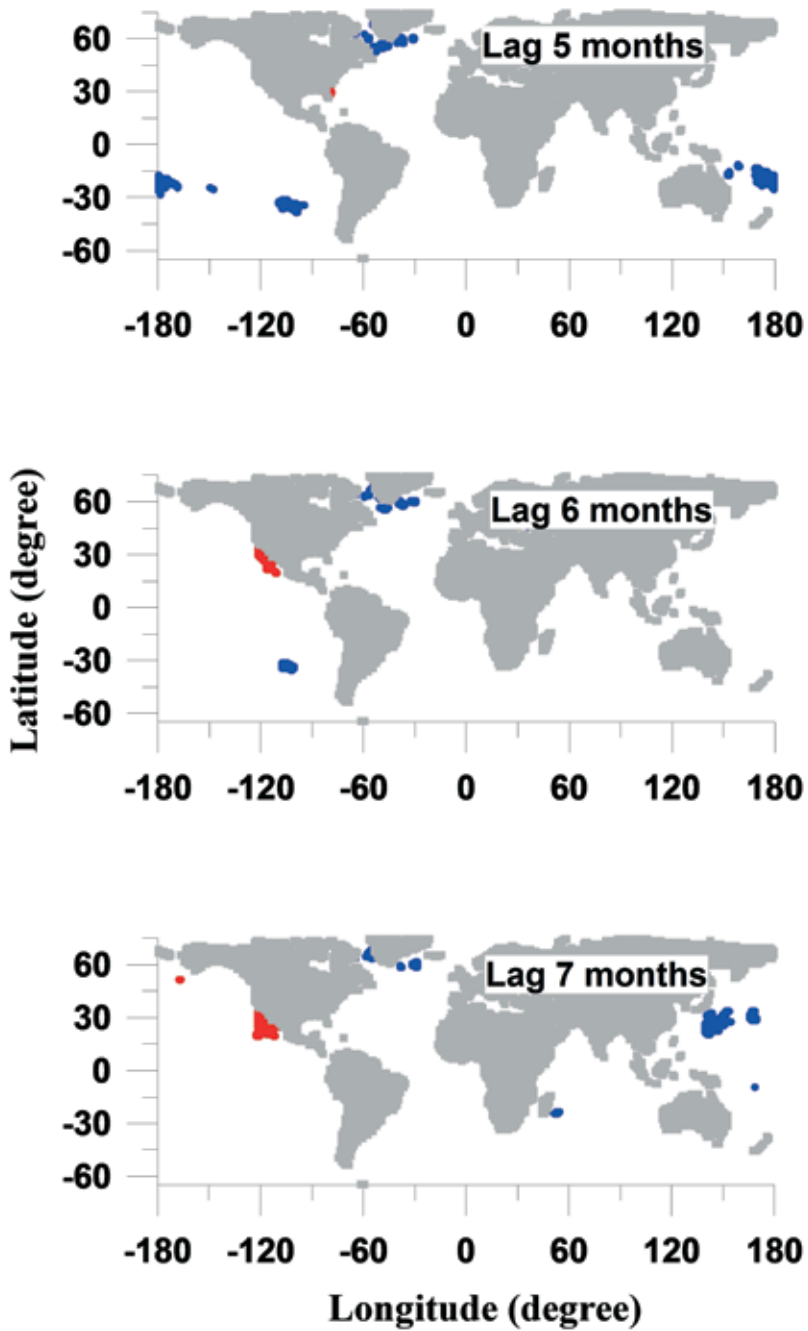


**Figure 6.** Significant SST areas for summer rainfall in all four vegetation zones ( $|r| > 0.33$ ). Red and blue colors indicate positive and negative correlations, respectively.

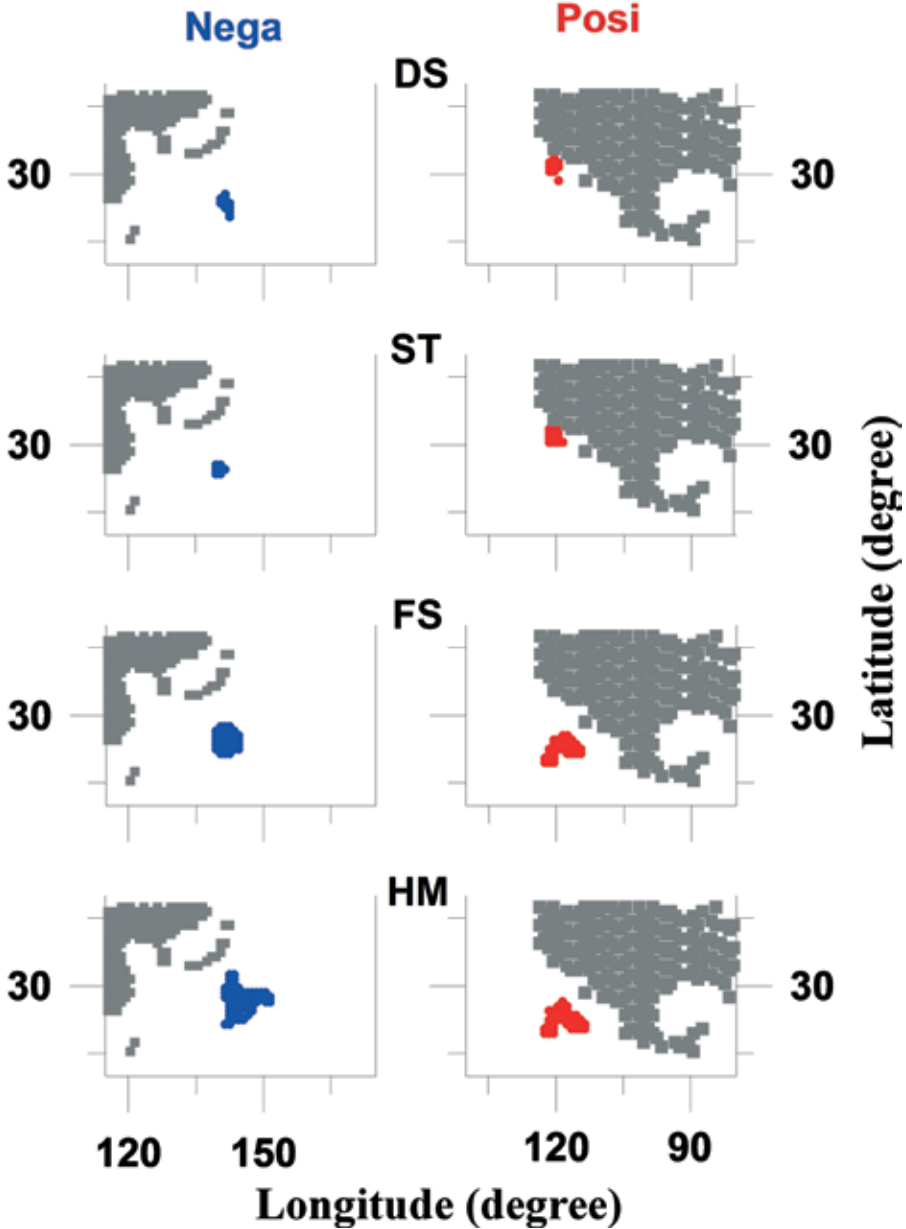


**Figure 7.** A significant SST dipole for summer rainfall that occurs for all four vegetation zones (lag 7 months). Red and blue colors indicate positive and negative correlations, respectively.

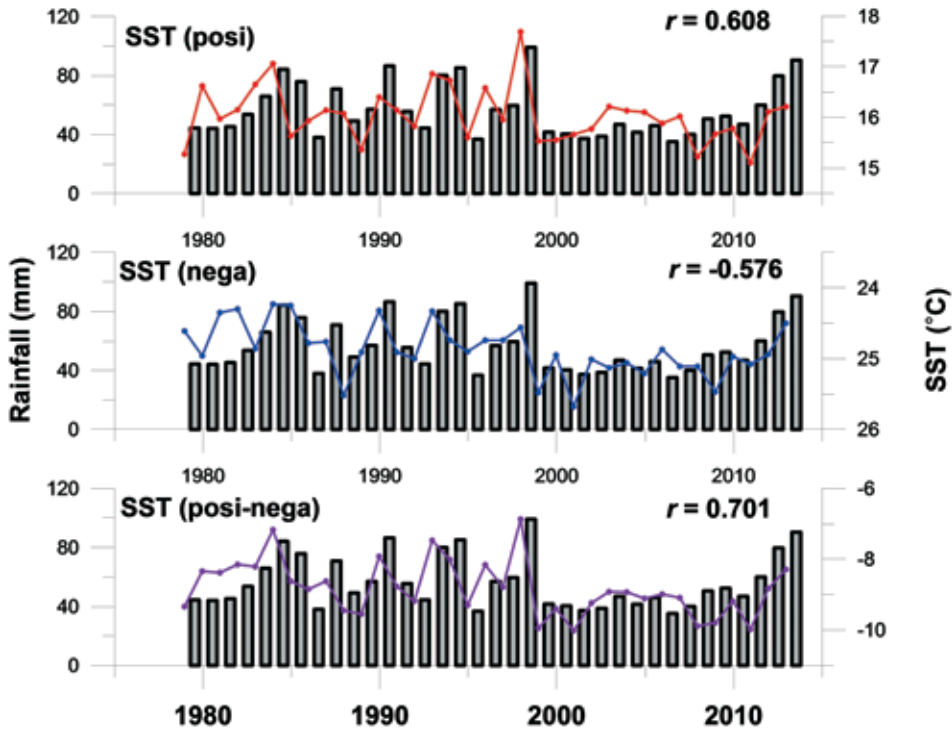


**Figure 8.** Time series of SST and ST summer rainfall (ST summer rainfall lags SST by 7 months).

(Fig. 8, bottom) is 0.70. Table 1 shows the correlations of the SST dipole corresponding to Fig. 8. The correlation for the time series of the difference is 9–13% stronger than the original positive and negative time series.

### 5. Prediction of summer rainfall using SST dipoles

The strong SST dipole identified above was used to predict the summer rainfall for the four vegetation zones in Mongolia. Because the SST dipole was strongly correlated with the Mongolian summer rainfall, we tested the prediction of summer rainfall 7 months in advance using an ANN model. The SST and

*Table 1. Comparison of prediction results using positively and negatively correlated SSTs as compared to using the SST dipole (Posi-Nega).*

	ST	ST	FS	HM
Positive	0.449	0.608	0.581	0.473
Negative	-0.487	-0.576	-0.637	-0.534
Posi-Nega	0.544	0.701	0.706	0.576

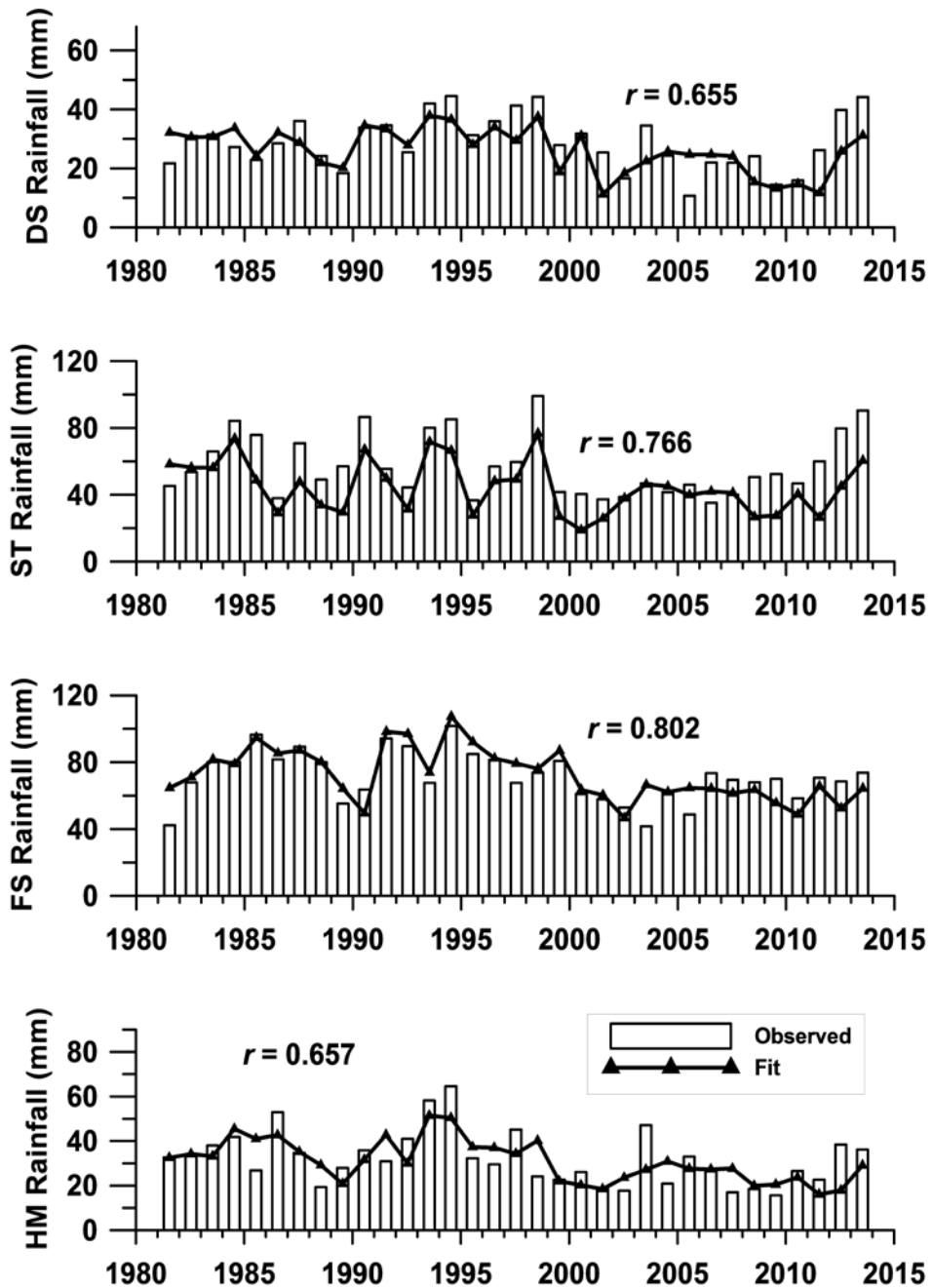


Figure 9. Observed summer rainfall (JJA) and the prediction 7 months ahead of time for the four vegetation zones.

rainfall data for the first 18 years (1979–1996) were used as calibration, and data from the following 17 years (1997–2013) were used to verify the model (*e.g.*, Singh and Borah, 2013). As described above, the weights of the model were optimized by back propagation. The results were in good agreement (Fig. 9). The correlations between the observed and predicted summer rainfall for DS, ST, FS, and HM were 0.66, 0.77, 0.80, and 0.66, respectively. In statistical terms, the significance levels of 0.05, 0.01 and 0.001 correspond to correlations of 0.33, 0.43, and 0.53, respectively. This result indicates that the SST dipole in the Pacific Ocean may enable accurate prediction of Mongolian summer rainfall 7 months ahead of time.

## 6. Conclusions

1. The inter-annual time series of summer rainfall (JJA) for the four vegetation zones (DS, ST, FS, and HM) in Mongolia display high and significant correlation with earlier months' SST in various areas over the oceans. In particular, the summer rainfall of FS and HM showed strong correlation with large SST areas.

2. Pairs of SST areas of dipoles are significantly positively and negatively correlated with the summer rainfall.

3. The SST difference between the poles of a dipole which measures its strength showed higher correlation with the summer rainfall than the separated SST correlations.

4. Common SST areas significantly correlated with the summer rainfall of all four Mongolian vegetation zones are located off the south coast of Greenland in the Atlantic Ocean at time lags of 5, 6, and 7 months.

5. For a lag of 7 months, an SST dipole off the west coast of North America (positive) and south of Japan (negative) in the Pacific Ocean is correlated with summer rainfall of the four vegetation zones.

6. An ANN model was used for prediction of the summer rainfall by using the SST dipole difference in the Pacific Ocean 7 months prior to the rainy season. The agreement with observed and predicted summer rainfall was very good. The correlations between the predicted and observed summer rainfalls for the four vegetation zones (DS, ST, FS, and HM) were 0.66, 0.77, 0.80, and 0.66, respectively. This indicates that summer rainfall prediction using SST on both sides of the North Pacific Ocean can be beneficial for predictive purposes.

*Acknowledgements* – This study was carried out under the Joint Research Program of the Arid Land Research Center, Tottori University. This study was partially supported by the International Platform for Arid Land Research and Education, Tottori University and the Grant-in-Aid for Scientific Research (S) from JSPS “Integrating Dryland Disaster Science” (No.25220201).

## References

- Ahmed, A. O. C., Yasuda, H., Hattori, K. and Nagasawa, R. (2008): Analysis of rainfall records (1923–2004) in Atar-Mauritania, *Geofizika*, **25**, 53–64.
- Ashok, K, Guan Z. and Yamagata, T. (2001): Impact of the Indian Ocean Dipole on the between the Indian Monsoon Rainfall and ENSO, *Geophys. Res. Lett.*, **28**, 4499–4502, [DOI:10.1029/2001GL013294](https://doi.org/10.1029/2001GL013294).
- Behera, S. and Yamagata, T. (2001): Subtropical SST dipole events in the southern Indian Ocean, *Geophys. Res. Lett.*, **28**, 327–330, [DOI:10.1029/2000GL011451](https://doi.org/10.1029/2000GL011451).
- Biasutti, M. and Giannini, A. (2006): Sahel drying in response to late 20th century forcings, *Geophys. Res. Lett.*, **33**, L11706, [DOI:10.1029/2006GL026067](https://doi.org/10.1029/2006GL026067).
- Bishop, C. M. (1995): *Neural Network for Pattern Recognition*. Oxford University Press, New York, 504 pp.
- Camberlin, P. (1997): Rainfall anomalies in the source region of the Nile and their connection with the Indian summer monsoon, *J. Climate*, **10**, 1380–1392, [DOI:10.1175/1520-0442\(1997\)010<1380:RAITSR>2.0.CO;2](https://doi.org/10.1175/1520-0442(1997)010<1380:RAITSR>2.0.CO;2).
- Chiang, J. C. H., Fang, Y. and Chang, P. (2008): Interhemispheric thermal gradient and tropical Pacific climate, *Geophys. Res. Lett.*, **35**, L14704, [DOI:10.1029/2008GL034166](https://doi.org/10.1029/2008GL034166).
- Chung, C. E. and Ramanathan, V. (2007): Relationship between trends in land precipitation and tropical SST gradient, *Geophys. Res. Lett.*, **34**, L16809, [DOI:10.1029/2007GL030491](https://doi.org/10.1029/2007GL030491).
- Dash, N. B., Panda, S. N., Remesan, R. and Sahoo, N. (2010): Hybrid neural modeling for groundwater level prediction, *Neural Comput. Appl.*, **19**, 1251–1263, [DOI:10.1007/s00521-010-0360-1](https://doi.org/10.1007/s00521-010-0360-1).
- Davi, N. K., Jacoby, C., Ciritis, A. E. N. and Baatarbileg, N. (2006): Extension of drought records for Central Asia using tree rings: West-Central Mongolia, *J. Climate*, **19**, 288–299, [DOI:10.1175/JCLI3621.1](https://doi.org/10.1175/JCLI3621.1).
- Diro, G. T., Grimes, D. I. F. and Black, E. (2011): Teleconnections between Ethiopian summer rainfall and sea surface temperature: part I -observation and modeling, *Clim. Dynam.*, **37**, 103–119, [DOI:10.1007/s00382-010-0837-8](https://doi.org/10.1007/s00382-010-0837-8).
- Elagib, N. A. and Elhag, M. M. (2011): Major climate indicators of ongoing drought in Sudan, *J. Hydrol.*, **409**, 612–625, [DOI:10.1016/j.jhydrol.2011.08.047](https://doi.org/10.1016/j.jhydrol.2011.08.047).
- Fontaine, B., Gaetani, M., Ullman, A. and Roucou, P. (2011): Time evolution of observed July–September sea surface temperature Sahel climate teleconnection with removed quasi global effect (1900–2008), *J. Geophys. Res.*, **116**, D04105, [DOI:10.1029/2010JD014843](https://doi.org/10.1029/2010JD014843).
- Goulden, C. E., Nandintsetseg, B. and Ariuntsetseg, L. (2011): The geology, climate and ecology of Mongolia, in: *Mapping Mongolia: Situating Mongolia in the World from Geologic Time to the Present*, edited by Sabloff, Paula L.W. University of Pennsylvania Press, Philadelphia, 87–103, [DOI:10.9783/9781934536315.87](https://doi.org/10.9783/9781934536315.87).
- Goulden, C. E., Mead, J., Horwitz, R., Goulden, M., Nandintsetseg, B., McCormick, S., Boldgiv, B. and Petraitis, P. S. (2016): Interviews of Mongolian herders and high resolution precipitation data reveal an increase in short heavy rains and thunderstorm activity in semi-arid Mongolia, *Clim. Change*, **136**, 281–295, [DOI:10.1007/s10584-016-1614-4](https://doi.org/10.1007/s10584-016-1614-4).
- Goyal, M. K. and Ojha, C. S. P. (2012): Downscaling of surface temperature for lake catchment in an arid region in India using linear multiple regression and neural networks, *Int. J. Climatol.*, **32**, 552–566, [DOI:10.1002/joc.2286](https://doi.org/10.1002/joc.2286).
- Iizuka, S. and Matsuura, T. (2000): The Indian Ocean SST dipole simulated in a coupled general circulation model, *Geophys. Res. Lett.*, **27**, 3369 – 3372, [DOI:10.1029/2000GL011484](https://doi.org/10.1029/2000GL011484).
- Kumbuyo, C. P., Yasuda, H., Kitamura, Y. and Shimizu, K. (2014): Fluctuation of rainfall time series in Malawi: An analysis of selected areas, *Geofizika*, **31**, 13–34, [DOI:10.15233/gfz.2014.31.1](https://doi.org/10.15233/gfz.2014.31.1).

- Lee, E., Chasea, T. N. and Balaji, R. (2008): Seasonal forecasting of East Asian summer monsoon based on oceanic heat sources, *Int. J. Climatol.*, **28**, 667–678, [DOI:10.1002/joc.1551](https://doi.org/10.1002/joc.1551).
- Mahmud, M. and Kumar, T. S. V. (2008): Forecasting severe rainfall in the equatorial Southeast Asia, *Geofizika*, **25**, 109–128.
- Mantsis, D. F. and Clement, A. C. (2009): Simulated variability in the mean atmospheric meridional circulation over the 20th century, *Geophys. Res. Lett.*, **36**, L06704, [DOI:10.1029/2008GL036741](https://doi.org/10.1029/2008GL036741).
- Mondal, P., Srivastava, P., Kalin, L. and Panda, S. N. (2011): Ecologically sustainable surface water withdrawal for cropland irrigation through incorporation of climate variability, *J. Soil Water Conserv.*, **66**, 221–232, [DOI:10.2489/jswc.66.4.221](https://doi.org/10.2489/jswc.66.4.221).
- Morinaga, Y., Tian, S. F. and Shinoda, M. (2003): Winter snow anomaly and atmospheric circulation in Mongolia, *Int. J. Climatol.*, **23**, 1627–1636, [DOI:10.1002/joc.961](https://doi.org/10.1002/joc.961).
- Nagano, Y., Kato, H. and Yamanaka, S. (2009): Recent cooling trend over northern Japan in August in relation to the weakening of the Tibetan high, *J. Agric. Meteorol.* **65**, 129–139, [DOI:10.2480/agrmet.65.2.1](https://doi.org/10.2480/agrmet.65.2.1).
- Nandintsetseg, B. and Shinoda, M. (2011): Seasonal change of soil moisture in Mongolia: Its climatology and modeling, *Int. J. Climatol.*, **31**, 1143–1152, [DOI:10.1002/joc.2134](https://doi.org/10.1002/joc.2134).
- Nandintsetseg, B. and Shinoda, M. (2014): Multi-decadal soil moisture trends in Mongolia and their relationships to precipitation and evapotranspiration, *Arid Land Res. Manag.*, **28**, 247–260, [DOI:10.1080/15324982.2013.861882](https://doi.org/10.1080/15324982.2013.861882).
- Nandintsetseg, B. and Shinoda, M. (2015): Land surface memory effects on dust emission in a Mongolian temperate grassland, *J. Geophys. Res. Biogeosci.*, **120**, 414–427, [DOI:10.1002/2014JG002708](https://doi.org/10.1002/2014JG002708).
- Olsson, J, Uvo, C. B. and Jinno, K. (2001): Statistical atmospheric downscaling of short-term extreme rainfall by neural networks, *Phys. Chem. Earth Pt. B*, **26**, 695–700, [DOI:10.1016/S1464-1909\(01\)00071-5](https://doi.org/10.1016/S1464-1909(01)00071-5).
- Osman, Y. Z. and Shamseldin, A. Y. (2002): Qualitative rainfall prediction models for central and southern Sudan using El Nino - Southern Oscillation and Indian Ocean sea surface temperature indices, *Int. J. Climatol.*, **22**, 1861–1878, [DOI:10.1002/joc.860](https://doi.org/10.1002/joc.860).
- Rodriguez-Fonseca, B., Polo, I., Serrano, E. and Castro, M. (2006): Evaluation of the north Atlantic SST forcing on the European and Northern African winter climate, *Int. J. Climatol.*, **26**, 179–191, [DOI:10.1002/joc.1234](https://doi.org/10.1002/joc.1234).
- Saji, N. H., Goswami, B. N., Vinayachandran, P. N. and Yamagata, T. (1999): Dipole mode in the tropical Indian Ocean, *Nature*, **401**, 360–363, [DOI:10.1038/43855](https://doi.org/10.1038/43855).
- Shankar, D., Shetye, S. R. and Joseph, P. V. (2007): Link between convection and meridional gradient of sea surface temperature in the Bay of Bengal, *J. Earth Syst. Sci.*, **116**, 385–406, [DOI:10.1007/s12040-007-0038-y](https://doi.org/10.1007/s12040-007-0038-y).
- Shinoda, M., Ito, S., Nachinshonor, G. U. and Erdenetsetseg, D. (2007): Phenology of Mongolian grasslands and moisture conditions, *J. Meteorol. Soc. Jpn.*, **85**, 359–367, [DOI:10.2151/jmsj.85.359](https://doi.org/10.2151/jmsj.85.359).
- Singh, P. and Borah, B. (2013): Indian summer monsoon rainfall prediction using artificial neural network. *Stoch. Env. Res. Risk A*, **27**, 1585–1599, [DOI:10.1007/s00477-013-0695-0](https://doi.org/10.1007/s00477-013-0695-0).
- Smith, I. N., McIntosh, P., Ansell, T. J., Reason, C. J. C. and McInnes, K. (2000): Southwest western Australian winter rainfall and its association with ocean climate variability, *Int. J. Climatol.*, **20**, 1913–1930, [DOI:10.1002/1097-0088\(200012\)20:15<1913::AID-JOC594>3.0.CO;2-J](https://doi.org/10.1002/1097-0088(200012)20:15<1913::AID-JOC594>3.0.CO;2-J).
- Srivastava, P., McNair, J. N. and Johnson, T. E. (2006): Comparison of process-based and artificial neural network approaches for stream flow modeling in an agricultural watershed, *J. Am. Water Resour. As.*, **42**, 545–563, [DOI:10.1111/j.1752-1688.2006.tb04475.x](https://doi.org/10.1111/j.1752-1688.2006.tb04475.x).
- Srivastava, G., Panda, S. N., Mondal, P. and Liu, J. G. (2010): Forecasting of rainfall using ocean-atmospheric indices with a fuzzy neural technique, *J. Hydrol.*, **395**, 190–198, [DOI:10.1016/j.jhydrol.2010.10.025](https://doi.org/10.1016/j.jhydrol.2010.10.025).

- Sun, L., Shen, B. Z., Sui, B. and Huang, B. H. (2017): The influences of East Asian Monsoon on summer precipitation in Northeast China, *Clim. Dynam.*, **48**, 1647–1659, [DOI:10.1007/s00382-016-3165-9](https://doi.org/10.1007/s00382-016-3165-9).
- Uvo, C. B., Repelli, C. A., Zebiak, S. E. and Kushnir, Y. (1998): The relationships between tropical Pacific and Atlantic SST and northeast Brazil monthly precipitation, *J. Climate*, **11**, 551–562, [DOI:10.1175/1520-0442\(1998\)011<0551:TRBTPA>2.0.CO;2](https://doi.org/10.1175/1520-0442(1998)011<0551:TRBTPA>2.0.CO;2).
- Webster, P. J., Moore, A. M., Loschnigg, J. P. and Leben, R. R. (1999): Coupled oceanic-atmospheric dynamics in the Indian Ocean during 1997–98, *Nature*, **601**, 356–360, [DOI:10.1038/43848](https://doi.org/10.1038/43848).
- Yasuda, H., Berndtsson, R., Saito, T., Anyoji, H. and Zhang, X. (2009): Prediction of Chinese Loess Plateau summer rainfall using Pacific Ocean spring sea surface temperature, *Hydrol. Process.*, **23**, 719–729, [DOI:10.1002/hyp.7172](https://doi.org/10.1002/hyp.7172).
- Yu, L. and Rienecker, M. M. (1999): Mechanisms for the Indian Ocean warming during the 1997–98 El Niño, *Geophys. Res. Lett.*, **26**, 735–738, [DOI:10.1029/1999GL900072](https://doi.org/10.1029/1999GL900072).
- Zheng, J., Li, J. and Feng, J. A. (2014): Dipole pattern in the Indian and Pacific oceans and its relationship with the East Asian summer monsoon, *Environ. Res. Lett.*, **9**, 074006, [DOI:10.1088/1748-9326/9/7/074006](https://doi.org/10.1088/1748-9326/9/7/074006).

#### SAŽETAK

### Učinak oceanskog dipola površinske temperature mora (SST) na ljetnu oborinu u Mongoliji

*Hiroshi Yasuda, Banzragch Nandintsetseg, Ronny Berndtsson, Ganbat Amgalan, Masato Shinoda and Takayuki Kawai*

U svrhu predviđanja ljetne oborine izračunate su poprečne korelacije međugodišnjih vremenskih nizova ljetne oborine (od lipnja do kolovoza: JJA) za sušni dio Mongolije i globalne površinske temperature mora (GSST). Evaluirano je predviđanje ljetne oborine za četiri mongolske vegetacijske zone: pustinjska stepa (DS), stepa (ST), šumska stepa (FS) i visoko gorje (HM) pomoću GSST-a za vremenski odmak od 5, 6 i 7 mjeseci prije JJA oborine. Ljetna oborina u Mongoliji povezana je s globalnim SST-om. Konkretno, ljetna oborina u područjima FS i HM pokazala je visoku i statistički značajnu korelaciju sa SST-om u određenim dijelovima oceana. Identificirani su SST dipoli (parovi pozitivno i negativno koreliranih područja), a korelacija za vremenske nizove SST-a razlika između SST dipola (pozitivan – negativan) s ljetnim vremenskim nizovima kišnih kiša bila je veća od izvornih korelacija. Za predviđanje ljetnih oborina na temelju SST-a korišten je model neuronske mreže (ANN). Kao ulaz u ANN model korišteni su vremenski nizovi razlika SST-ova, koje odgovaraju snazi dipola, a ljetna oborina u Mongoliji predviđena je potom 5, 6 i 7 mjeseci unaprijed. Predviđena ljetna oborina dobro se slože s izmjerenom oborinom u četirima različitim vegetacijskim zonama. To podrazumijeva da se model može prilično uspješno koristiti za predviđanje ljetne oborine u četirima glavnim mongolskim vegetacijskim zonama s dobrom preciznošću.

**Ključne riječi:** umjetna neuronska mreža (ANN), suho tlo, oborina u Mongoliji, predviđanje oborine, SST telekonekcija